ARTICLE

DFT+U Analysis on Stability of Low-Index Facets in Hexagonal $LaCoO_3$ Perovskite: Effect of Co^{3+} Spin States

Dan Wu[a,b], Gong-dong Chen[a,b], Chao-yi Ge[a,b], Zhen-peng Hu[b,c*], Xue-hao He[d], Xin-gang Li[a,b*]

a. Tianjin Key Laboratory of Applied Catalysis Science & Technology (Tianjin), Tianjin 300072, China
b. Collaborative Innovation Center for Chemical Science & Engineering (Tianjin), Tianjin 300072, China
c. School of Physics, Nankai University, Tianjin 300071, China
d. Department of Chemistry, School of Science, Tianjin University, Tianjin 300072, China

(Dated: Received on March 16, 2017; Accepted on March 21, 2017)

By the first-principles calculations, most studies indicated that the $(1\bar{1}02)$-CoO_2 termination of $LaCoO_3$ cannot be stabilized, which disagrees with the experimental observation. Besides the crystal structure, we found that the spin states of Co^{3+} ions could affect surface stability, which previously were not well considered. By examining the different states of Co^{3+} ions in hexagonal-phase $LaCoO_3$, including low spin, intermediate spin, and high spin states, the surface grand potentials of these facets are calculated and compared. The results show that the spin states of Co^{3+} ions have an important influence on stability of the $LaCoO_3$ facets. Different from the previous results, the stability diagrams demonstrate that the $(1\bar{1}02)$-CoO_2 termination can stably exist under O-rich condition, which can get an agreement with the experimental ones. Furthermore, the surface oxygen vacancy formation energies (E_{O_v}) of stable facets are computed in different spin states. The E_{O_v} of these possible exposed terminations strongly depend on the spin state of Co^{3+} ions: in particular, the E_{O_v} of the HS states is lower than that of other spin states. This indicates that one can tune the properties of $LaCoO_3$ by directly tuning the spin states of Co^{3+} ions.

Key words: DFT+U, Spin state, Surface, Perovskite

I. INTRODUCTION

In recent decades, perovskite oxides (ABO_3) have aroused considerable interests as the cathode materials in solid oxide fuel cells for use in many energy storage and conversion technologies, such as the oxygen evolution reaction (OER) and oxygen reduction reaction (ORR) [1−5]. These oxides are also catalytically-active and cost-effective catalysts for many important chemical reactions, such as NO_x (including NO and NO_2) storage reduction [6, 7], CO oxidation [8], and methane combustion [9]. Since those catalytic reactions are surface processes, studies on the surface properties of those materials play an important role in deeply understanding the catalytic reactions. Usually, the experimental observations believed that (001) facets, particularly (001) B-terminated surface, in perovskite oxides (ABO_3) are stable and play a pivotal role in these catalytic chemical reactions [10−14]. However, to the best of our knowledge, the surface stabilities of perovskite oxides, especially for $LaCoO_3$, are still under debate from theoretical calculations. For example, using the cubic-phase structure of $LaCoO_3$ in the calculations, Kahn *et al.* [15] predicted the Co-terminated (111) surface and LaCoO-terminated (110) surface to be the most stable; Chen *et al.* [16] reported that the ground termination was the (001)-LaO surface, transitioning to the (111)-LaO_3 facet in oxygen-rich condition; while Zhang *et al.* [17] found that the LaO- and CoO_2-terminated (001) surfaces were stable.

It is noticed that $LaCoO_3$ has a rhombohedral primitive cell with $R\bar{3}c$ symmetry [18−23], which belongs to the hexagonal phase, but the cubic phase was used in the previous calculations [15−17]. As well known, results from the first-principles calculations are very sensitive to the geometric structure of materials. Therefore, the complexity of previous studies may come from the difference on crystal structures of $LaCoO_3$. Recently, Liu *et al.* explored the stability of low-index facets on the hexagonal-phase $LaCoO_3$ by using the first-principles analysis [24], and they found that the $(1\bar{1}02)$-LaO, $(\bar{1}104)$-O_2 and (0001)-LaO_3 terminations were thermodynamically stable with a non-spin (NS) state. Though a more accurate crystal structure was employed in their calculations, the results were still in conflict with the common sense from the experimentalists that the (001)-CoO_2 was stable and active in the reactions [11−14]. There might be some key factors ig-

*Authors to whom correspondence should be addressed. E-mail: zphu@nankai.edu.cn, xingang_li@tju.edu.cn

noredin previous calculations, which can reconcile the disagreement between computational result and experimental observation.

Besides the crystal structure, the spin state of Co^{3+} ion is another important factor which can affect the results of calculations, but was not well considered before. As reported in Ref.[25−29], $LaCoO_3$ exhibits nonmagnetic behavior at low temperature (below 90 K) where the Co^{3+} ions are in the low spin (LS) states, and undergoes a transition from semiconductor to metal over 500 K, coincident to the spin state transition from intermediate spin (IS) to high spin (HS). It has also been reported that the spin states of Co^{3+} ions in $LaCoO_3$ can greatly affect oxygen vacancy formation on the surface [30] and their migration in the bulk [31]. However, there is a lack of report on surface stability of $LaCoO_3$ with consideration of the effects of spin states of Co^{3+} ions. To this point, the reason for the above disagreement may arise from the spin states of the Co^{3+} ions in $LaCoO_3$. It is necessary to perform calculations with appropriate Co^{3+} spin states to clarify the properties of $LaCoO_3$ surface systems for the in-depth researches.

In this work, we compared the surface grand potentials (Ω) of low-index facets of hexagonal-phase $LaCoO_3$, where the Co^{3+} ions' spin states are in LS, IS (ferromagnetic (FM), and anti-ferromagnetic (AFM)) and HS (FM, and AFM) states, to get a comprehensive understanding of $LaCoO_3$ surface systems. We determined the stable surfaces of $LaCoO_3$ in special chemical conditions by comparing the surface grand potentials (Ω). As the spin states of Co^{3+} ions change, the region of stability diagram undergoes a significant variation. In addition, the E_{O_v} of stable facets of $LaCoO_3$ were computed in different spin states. It indicates that the energy of surface oxygen vacancy links strongly to the spin moment of Co^{3+} ions. Our simulations indicate that the $(1\bar{1}02)$-CoO_2-terminated facet in hexagonal $LaCoO_3$ can be stabilized in most spin states when the Co^{3+} ions' spin states are taken into consideration. And this agrees well with the experimental observation.

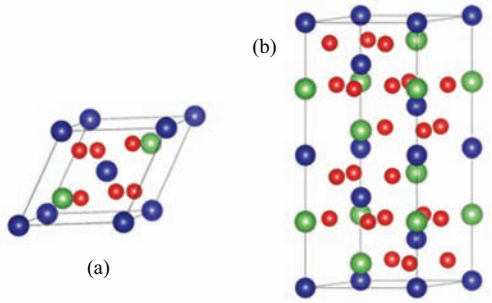

FIG. 1 (a) Rhombohedral primitive cell and (b) hexagonal unit cells of $LaCoO_3$. Green, blue, and red balls represent La, Co and O atoms, respectively.

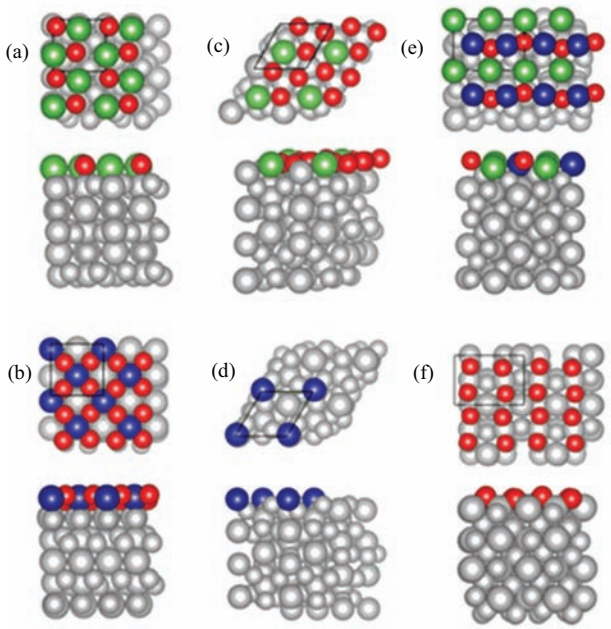

FIG. 2 The top and side views of optimized (a) $(1\bar{1}02)$-LaO, (b) $(1\bar{1}02)$-CoO_2, (c) (0001)-LaO_3, (d) (0001)-Co, (e) $(\bar{1}104)$-LaCoO, and (f) $(\bar{1}104)$-O_2. Green, blue, and red balls represent La, Co, and O atoms, respectively.

II. COMPUTATIONAL DETAILS

A. Models of bulk and slab

The space group of crystalline $LaCoO_3$ is $R\overline{3}c$ (No.167), which can be constructed with either a rhombohedral or a hexagonal model (FIG. 1). The Jahn-Teller effect causes a slight distortion of CoO_6 octahedron in $LaCoO_3$, resulting in a primitive cell of rhombohedral structure [18] with lattice parameters of a=b=c=5.344 Å, α=β=γ=61.01° (FIG. 1(a)). As shown in FIG. 1(b), the experimental lattice parameters of hexagonal model [18] are a=b=5.426 Å, c=12.991 Å, α=β=90°, and γ=120°.

In order to discuss the thermodynamic stability of the low-index surfaces, we constructed six slab models. Adapted from the models in Ref.[24], a seven-layer nonstoichiometric slab of LaO (FIG. 2(a)) or CoO_2 (FIG. 2(b)) termination was used to simulate the facet along the $(1\bar{1}02)$ direction, a thirteen-layer nonstoichiometric slab of LaO_3 (FIG. 2(c)) or Co (FIG. 2(d)) termination was used to simulate the facet along the (0001) direction; and an eleven-layer nonstoichiometric slab of LaCoO (FIG. 2(e)) or O_2 (FIG. 2(f)) termination was used to simulate the facet along the $(\bar{1}104)$ direction. The $(1\bar{1}02)$, (0001) and $(\bar{1}104)$ directions in the hexagonal phase correspond to the (001), (111) and (110) directions in a pseudo cubic phase. The black frames in FIG. 2 represent the periodic boundaries.

DOI:10.1063/1674-0068/30/cjcp1703035

B. General setup for computation

Density functional theory (DFT) calculations were performed with the Vienna *ab initio* Simulation Package (VASP) [32, 33]. The nuclei and core electrons were treated with the projector augmented wave (PAW) [34] method. Generalized gradient approximation (GGA) with the Perdew-Burke-Ernzerhof (PBE) [35] form was employed to describe the electron exchange and correlation. For relaxation of bulk $LaCoO_3$ (hexagonal phase), a plane wave basis set with cut-off of 400 eV and a 7×7×3 Monkhorst-Pack [36] k-point mesh were used to get the optimal lattice parameters. The optimal parameters of hexagonal phase are a=b=5.485 Å and c=13.031 Å. For the slab calculations, the plane wave energy cutoff of 400 eV and a 3×3×1 of k-point mesh were used to get the properties of different surfaces. All the atoms in the bulk and slab were allowed to relax until the maximum force on each atom was smaller than 0.05 eV/Å. In each slab model, a separation over 15 Å in vacuum was introduced to minimize interactions between periodic images.

The oxygen vacancy formation energy (E_{O_v}) is calculated using the following equation:

$$E_{O_v} = E(\text{defect}) - E(\text{perfect}) + \frac{1}{2}E(O_2) \quad (1)$$

where E(defect) is the total energy of the slab with one surface oxygen vacancy, E(perfect) is the energy of the ideal slab and $E(O_2)$ is the energy of the O_2 molecule in the gas phase, respectively.

The different Co-3d occupations result in three spin states of Co^{3+} ions in $LaCoO_3$, including LS of $t_{2g}{}^6e_g{}^0$ (S=0), IS of $t_{2g}{}^5e_g{}^1$ (S=1) and HS of $t_{2g}{}^4e_g{}^2$ (S=2). Each spin state was constructed by changing the initial magnetic moment of Co^{3+} ion, *i.e.* LS=0, IS=±2 and HS=±4, where the quantity is the difference between alpha and beta electrons in a certain Co^{3+} ion. The initial configurations of all Co^{3+} ions were set by MAGMOM, and then NUPDOWN was chosen to control the total spin of the slab. The selection rule of spin was also applied to get a reasonable energy when oxygen vacancy was generated. For example, two total spin numbers of the defect slab (+2 or −2 from the total spin number of initial slab) were calculated and the lower energy was accepted. The spin state of calculated O_2 molecule is always triplet. The partially filled d states in the Co^{3+} ions are not well described by the standard DFT calculations, where the normal GGA methods give a zero band gap of $LaCoO_3$ on the contrast to the experimental value of about 0.6 eV [37]. We thus performed the DFT+U approach, where the on-site U and J were treated as a single effective parameter among the d electrons on the Co^{3+} ions, U_{eff}=U−J [38−40]. We fixed J=0.49 eV [41] in all our GGA+U calculations, and varied the value of U in determining an optimal parameter U (3.4 eV), which will be discussed later.

C. The surface grand potential

To compare the stability of different terminations, the surface grand potential (Ω) is implemented in the calculations, as defined in Ref.[42]

$$\Omega = \frac{1}{2S}\left(E_{\text{slab}} - N_{\text{La}}\mu_{\text{La}} - N_{\text{Co}}\mu_{\text{Co}} - N_{\text{O}}\mu_{\text{O}}\right) \quad (2)$$

where N_{La}, N_{Co}, and N_{O} are the numbers of La, Co, and O atoms in the slab, respectively, and μ represents the chemical potential of La, Co, and O atoms species. Since the surface is in thermodynamic equilibrium with the bulk $LaCoO_3$ (μ_{LaCoO_3}=$E^{\text{bulk}}_{LaCoO_3}$) and the chemical potentials of each species are related to the chemical potential of the bulk crystal, we thus have the following constraint:

$$E^{\text{bulk}}_{LaCoO_3} = \mu_{LaCoO_3} = \mu_{\text{La}} + \mu_{\text{Co}} + 3\mu_{\text{O}} \quad (3)$$

When μ_{La} is eliminated by Eq.(2) and (3), we introduce:

$$\Delta\mu_{\text{Co}} = \mu_{\text{Co}} - E^{\text{bulk}}_{\text{Co}} \quad (4)$$

$$\Delta\mu_{\text{O}} = \mu_{\text{O}} - \frac{1}{2}E^{\text{mol}}_{O_2} \quad (5)$$

Subsequently, the surface grand potential can be determined as:

$$\Omega = \phi - \frac{1}{2S}\left[\Delta\mu_{\text{O}}(N_{\text{O}} - 3N_{\text{La}}) + \Delta\mu_{\text{Co}}(N_{\text{Co}} - N_{\text{La}})\right] \quad (6)$$

$$\phi = \frac{1}{2S}\left[E_{\text{slab}} - N_{\text{La}}E^{\text{bulk}}_{LaCoO_3} - \frac{E^{\text{mol}}_{O_2}}{2}(N_{\text{O}} - 3N_{\text{La}}) - E^{\text{bulk}}_{\text{Co}}(N_{\text{Co}} - N_{\text{La}})\right] \quad (7)$$

The surface La, Co, and O atoms are assumed to form no condensate on the surface, and the chemical potential of each species must be lower than the energy of an atom in the stable phase. We thus obtain the following upper limits of the chemical potentials:

$$\Delta\mu_{\text{O}} = \mu_{\text{O}} - \frac{1}{2}E^{\text{mol}}_{O_2} < 0 \quad (8)$$

$$\Delta\mu_{\text{La}} = \mu_{\text{La}} - E^{\text{bulk}}_{\text{La}} < 0 \quad (9)$$

$$\Delta\mu_{\text{Co}} = \mu_{\text{Co}} - E^{\text{bulk}}_{\text{Co}} < 0 \quad (10)$$

By combining Eq.(3) and (9), the lower limits can be determined as follows,

$$\Delta\mu_{\text{Co}} + 3\Delta\mu_{\text{O}} > -E^{\text{f}}_{LaCoO_3} \quad (11)$$

$$-E^{\text{f}}_{LaCoO_3} = E^{\text{bulk}}_{LaCoO_3} - E^{\text{bulk}}_{\text{La}} - E^{\text{bulk}}_{\text{Co}} - \frac{3}{2}E^{\text{mol}}_{O_2} \quad (12)$$

where $E^{\text{f}}_{LaCoO_3}$ is the formation energy of $LaCoO_3$ bulk crystal with respect to the La and Co atoms in their bulk phases, and the O atom in the gas phase. Once $\Delta\mu_{\text{Co}}$ and $\Delta\mu_{\text{O}}$ are determined in the effective ranges, the accessible values of Ω are thus obtained.

DOI:10.1063/1674-0068/30/cjcp1703035

III. RESULTS AND DISCUSSION

A. Determining the optimized U parameter

It is well known that U parameter plays an important role in the determination of the valence structure and the crystal structure. Since the band gap is generally related to the electronic structure of the bulk $LaCoO_3$, it is essential to determine an appropriate U value for Co element to correct the mistake. Previous studies indicate that the ground state $LaCoO_3$ is a nonmagnetic semiconductor with Co^{3+} ions in the LS state [28, 29]. Therefore, band gap scan calculations were performed with the parameter U varying from 2.9 eV to 3.9 eV with an interval of 0.1 eV on the LS ground state. The band gap as a function of the exchange parameter U is shown in FIG. 3. With the increase of parameter U, the value of the band gap linearly increases. When U=3.4 eV is employed, a band gap of 0.61 eV is obtained, which well agrees with the experimental value [37]. The U parameter of 3.4 eV was thus used for the GGA+U calculations to investigate surface stability of $LaCoO_3$ perovskite.

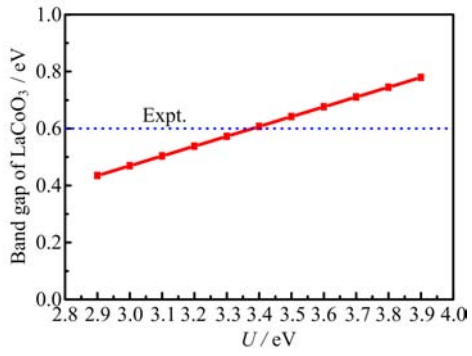

FIG. 3 Band gap of hexagonal phase $LaCoO_3$ as a function of exchange parameter U.

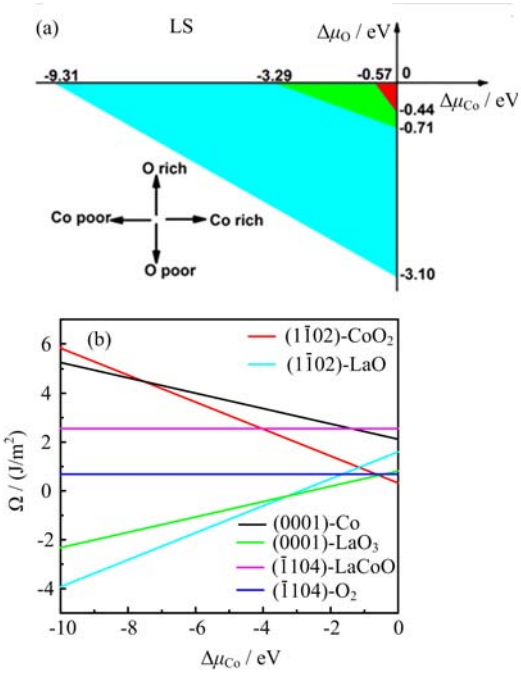

FIG. 4 (a) Stability diagram of the low-index surfaces of hexagonal $LaCoO_3$ in LS state. The surface grand potential (Ω) is represented as functions of $\Delta\mu_{Co}$ and $\Delta\mu_O$. (b) The surface grand potentials of different terminations in condition of $\Delta\mu_O$=0 eV.

B. Thermodynamic stability in different spin states with GGA+U

To examine the influence of spin states of Co^{3+} ions on surface stability, the surface grand potentials (Ω) of low-index facets have been calculated (Table S1−S3 in supplementary materials), where the Co^{3+} ions' spin states are in LS, IS (FM, AFM) and HS (FM, AFM) states, respectively. The FM and AFM configurations can be considered as two limits in energy with respect to the spin state of $LaCoO_3$. To determine the accessible values of Ω, we should calculate the effective intervals of $\Delta\mu_{Co}$ and $\Delta\mu_O$ according to the formation energy of $LaCoO_3$ bulk crystal, as defined in Ref.[42]. The obtained formation energy of hexagonal $LaCoO_3$ is −9.31 eV. On the basis of Eq.(11), $\Delta\mu_{Co}$ and $\Delta\mu_O$ are thus restricted within the ranges of (−9.31 eV<$\Delta\mu_{Co}$<0.00 eV) and (−3.10 eV<$\Delta\mu_O$< 0.00 eV), respectively.

The stability diagram of the surface grand potential Ω of different terminations within the allowed area is displayed in FIG. 4(a) when the Co^{3+} ions are in LS state. Only three terminations out of six low-index facets are found to be stable: (1$\bar{1}$02)-LaO, (0001)-LaO_3 and (1$\bar{1}$02)-CoO_2. The calculated results indicate that the (1$\bar{1}$02)-LaO termination is stable in low O chemical potential and low Co chemical potential, while its complementary, the (1$\bar{1}$02)-CoO_2 termination is in rich O chemical potential and rich Co chemical potential. Additionally, the (0001)-LaO_3 facet shows a stability domain in moderate Co and rich O environment. FIG. 4(b) reveals the Ω of different facets of the low spin Co^{3+} ions as a function of $\Delta\mu_{Co}$ with $\Delta\mu_O$=0 eV. It can be noted that the (1$\bar{1}$02)-LaO termination is favored in a large interval (−9.31 eV<$\Delta\mu_{Co}$ <−3.29 eV) and the (1$\bar{1}$02)-CoO_2 termination becomes stable in a small interval (−0.57 eV<$\Delta\mu_{Co}$<0 eV). When $\Delta\mu_{Co}$ is restricted to (−3.29 eV<$\Delta\mu_{Co}$<−0.57 eV), only the (0001)-LaO_3 termination can be observed.

FIG. 5(a) shows the Ω of different terminations as functions of $\Delta\mu_{Co}$ and $\Delta\mu_O$ in IS state with a FM configuration. Our calculations suggest that (1$\bar{1}$02)-CoO_2, (0001)-Co and ($\bar{1}$104)-LaCoO are unstable because their surface grand potentials are always larger than that of at least one stable facet within the allowed region. According to FIG. 5(a), the (1$\bar{1}$02)-LaO termination is the most stable one in O- and Co-poor conditions. The

DOI:10.1063/1674-0068/30/cjcp1703035

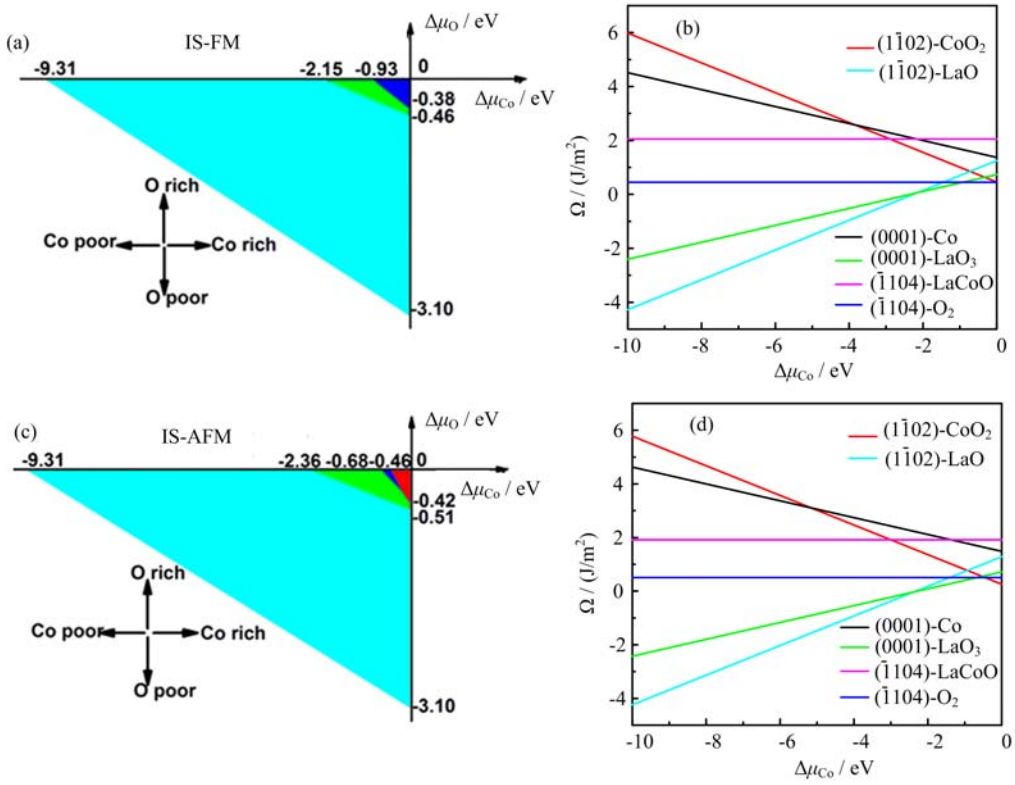

FIG. 5 (a) and (c) Stability diagram of the low-index surfaces of hexagonal $LaCoO_3$ in IS state with a FM and an AFM configurations. The surface grand potential (Ω) is represented as functions of $\Delta\mu_{Co}$ and $\Delta\mu_O$. (b) and (d) The surface grand potentials of different terminations in condition of $\Delta\mu_O$=0 eV in IS state with a FM and an AFM configurations.

(0001)-LaO_3 and ($\bar{1}$104)-O_2 terminations are favored in a small region corresponding to O- and Co-rich environments, respectively. FIG. 5(b) shows the Ω of different facets as a function of $\Delta\mu_{Co}$ in O-rich condition ($\Delta\mu_O$=0 eV) in IS state with a FM configuration. It appears that the (0001)-LaO_3 and ($\bar{1}$104)-O_2 terminations can be stabilized in a very limited area (-2.15 eV $<\Delta\mu_{Co}<-0.93$ eV and -0.93 eV$<\Delta\mu_{Co}<0$ eV), respectively. When $\Delta\mu_{Co}$ is lower than -2.15 eV, only the (1$\bar{1}$02)-LaO termination can be observed.

As displayed in FIG. 5(c), the (1$\bar{1}$02)-LaO, (0001)-LaO_3, ($\bar{1}$104)-O_2 and (1$\bar{1}$02)-CoO_2 are thermodynamically most favorable when the IS state is in an AFM configuration. Compared to the stability diagram of the IS state with a FM configuration, the area of the (1$\bar{1}$02)-LaO and (0001)-LaO_3 facets hardly change, while the region of ($\bar{1}$104)-O_2 termination only exists in a very small domain. The (1$\bar{1}$02)-CoO_2 termination emerges and becomes most stable in rich O and Co environment. FIG. 5(d) plots the surface grand potential Ω of different facets as a function of $\Delta\mu_{Co}$ with $\Delta\mu_O$=0 eV in IS state with an AFM configuration. The (1$\bar{1}$02)-LaO termination is favorable in a large interval (-9.31 eV $<\Delta\mu_{Co}<-2.36$ eV). For the complementary termination, the (1$\bar{1}$02)-CoO_2 can be stabilized in a small interval (-0.46 eV$<\Delta\mu_{Co}<0$ eV). When $\Delta\mu_{Co}$ is restricted to (-2.36 eV$<\Delta\mu_{Co}<-0.46$ eV), two stable terminations, the (0001)-LaO_3 and ($\bar{1}$104)-O_2 terminations, can be obtained.

FIG. 6(a) plots the surface grand potential Ω of different terminations as functions of $\Delta\mu_{Co}$ and $\Delta\mu_O$ in HS state with a FM configuration. The calculated results indicate that only four terminations are thermodynamically stable: (1$\bar{1}$02)-LaO, (0001)-LaO_3, ($\bar{1}$104)-O_2 and (1$\bar{1}$02)-CoO_2 as shown in FIG. 6(a). The (1$\bar{1}$02)-LaO termination is stable at low O chemical potential (O-poor limit) and low Co chemical potential (Co-poor limit), as the (0001)-LaO_3 facet shows a stability domain in moderate Co and rich O environment. In general, the ($\bar{1}$104)-O_2 and (1$\bar{1}$02)-CoO_2 terminations become the stable facets in a small domain corresponding to Co- and O-rich conditions. FIG. 6(b) plots the Ω of different facets of the high spin Co^{3+} ions with a FM configuration as a function of $\Delta\mu_{Co}$ with $\Delta\mu_O$=0 eV (O-rich condition). The results indicate that when $\Delta\mu_{Co}$ ranges from -9.31 eV to -4.60 eV, the (1$\bar{1}$02)-LaO termination is favored. When $\Delta\mu_{Co}$ is restricted to (-4.60 eV $<\Delta\mu_{Co}<-0.98$ eV), only the (0001)-LaO_3 surface can be observed. When $\Delta\mu_{Co}$ increases to -0.45 eV, the (1$\bar{1}$02)-O_2 termination disappears and the (1$\bar{1}$02)-CoO_2 surface emerges. Notably, these (0001)-Co and ($\bar{1}$104)-LaCoO terminations cannot be stabilized because they are outside of the accessible region.

DOI:10.1063/1674-0068/30/cjcp1703035

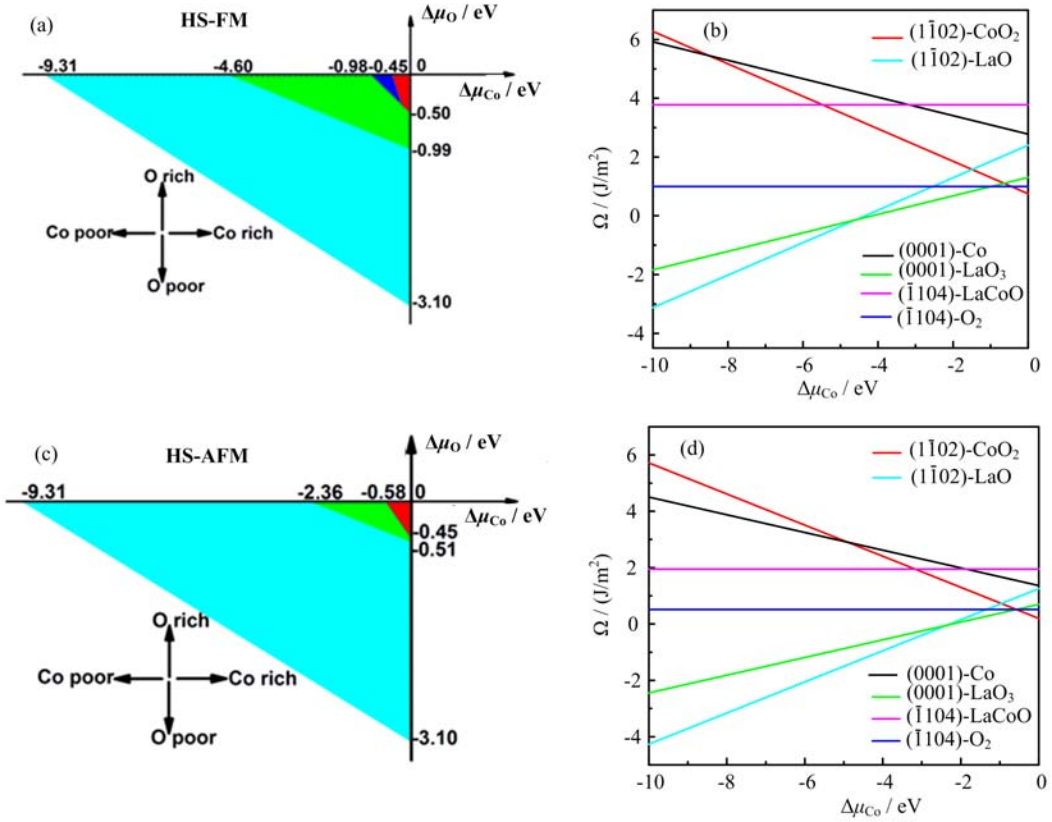

FIG. 6 (a) and (c) Stability diagram of the low-index surfaces of hexagonal $LaCoO_3$ in HS state with a FM and an AFM configurations. The surface grand potential (Ω) is represented as functions of $\Delta\mu_{Co}$ and $\Delta\mu_O$. (b) and (d) The surface grand potentials of different terminations in condition of $\Delta\mu_O$=0 eV in HS state with a FM and an AFM configurations.

As shown in FIG. 6(c), when the HS state is in the AFM configuration, the (1$\bar{1}$02)-LaO, (0001)-LaO_3 and (1$\bar{1}$02)-CoO_2 terminations are the most favorable facets. The stable region of (1$\bar{1}$02)-LaO termination of the AFM configuration is larger than that of the FM configuration. However, the area of (0001)-LaO_3 becomes smaller. And the (1$\bar{1}$02)-CoO_2 facet almost does not change. FIG. 6(d) reveals the Ω of the lowest-energy facets of the high spin Co^{3+} ions with an AFM configuration as a function of $\Delta\mu_{Co}$ in O-rich condition ($\Delta\mu_O$=0 eV). According to FIG. 6(d), the ($\bar{1}$104)-LaCoO, (0001)-Co and ($\bar{1}$104)-O_2 facets cannot be obtained; however, the (1$\bar{1}$02)-LaO, (0001)-LaO_3 and (1$\bar{1}$02)-CoO_2 terminations can be stabilized in some special Co environment, as -9.31 eV$<\Delta\mu_{Co}<-2.36$ eV, -2.36 eV$<\Delta\mu_{Co}<-0.58$ eV, and -0.58 eV$<\Delta\mu_{Co}<0$ eV, respectively.

According to the above calculations, as the Co^{3+} ions' spin states change, the stability diagram of low-index facets in hexagonal-phase $LaCoO_3$ undergoes a significant variation. Considering different spin states of Co^{3+} ions and different magnetic configurations, one can find that (1$\bar{1}$02)-LaO termination is stable in a large region with oxygen poor condition. Moreover, the (0001)-LaO_3 and (1$\bar{1}$02)-CoO_2 terminations can be stabilized in an oxygen rich condition, which is a typical experimental environment for $LaCoO_3$. And tuning the chemical potential of Co can tune the final surface exposition of $LaCoO_3$ nanoparticle. The (1$\bar{1}$02)-CoO_2 termination is favorable under suitable chemical potential regions, which can reach an agreement on theoretical results and experimental observation. This corresponds to the spin states of Co^{3+} ions in perovskite $LaCoO_3$. The Co^{3+} ions occupying octahedral sites surrounded by oxygen ions can introduce complex magnetic property in $LaCoO_3$, which has influence on the Co−O and O−O bond strength on the surface.

C. Oxygen vacancy formation energy of the stable facets

Surface oxygen vacancy plays a key role in the catalytic oxidation reactions in perovskite $LaCoO_3$. We therefore analyze how the spin states of Co^{3+} ions change the fundamental properties of oxygen vacancy formation. In order to explore the properties of these possible exposed facets, the E_{O_v} of the surfaces have been calculated. As shown in Table I, it can be found that higher Co^{3+} magnetic moments lead to lower oxygen vacancy formation energies, in good agreement with the previous work [30]. They attribute the tendencies in the surface oxygen vacancy formation energies to varia-

DOI:10.1063/1674-0068/30/cjcp1703035

TABLE I Oxygen vacancy formation energy (E_{O_v}) for possible exposed surfaces with different spin configurations.

Surface	E_{O_v}/eV		
	$(1\bar{1}02)$-LaO	(0001)-LaO_3	$(1\bar{1}02)$-CoO_2
LS	4.29	1.14	1.51
IS-FM	3.34	1.00	0.85
IS-AFM	4.76	0.74	1.22
HS-FM	1.70	0.20	0.08
HS-AFM	4.14	0.69	1.05
NS	4.69	0.68	1.24
NS [24]	4.38	0.09	–

tions in the O p-band center, which can be described as the Co−O bond strength. This trend suggests that oxygen vacancy energetics link strongly to the spin moment of Co^{3+} ions. Furthermore, whether the Co^{3+} ions are in a LS, an IS-FM, an IS-AFM, a HS-FM or a HS-AFM configuration, the $(1\bar{1}02)$-LaO termination has the highest E_{O_v} among these surfaces. It indicates that the $(1\bar{1}02)$-LaO facet may be not active, since O atoms are strongly bound. In the HS-FM configuration, the E_{O_v} of $(1\bar{1}02)$-CoO_2 termination is close to zero (0.08 eV), which is lower than that of (0001)-LaO_3 termination (0.20 eV). When the spin state of Co^{3+} ions is in a HS-AFM configuration, the E_{O_v} of $(1\bar{1}02)$-CoO_2 facet is 1.05 eV, which is more than the (0001)-LaO_3 termination (0.69 eV). As a result, it can be predicted that the $(1\bar{1}02)$-CoO_2- and (0001)-LaO_3-terminated surfaces might have good activity of O atoms, which can play a critical role in the surface reaction processes.

For comparison, we also calculated surface oxygen vacancy formation energies with NS polarized method as used in Ref.[24]. The NS oxygen vacancy formation energy of the $(1\bar{1}02)$-LaO termination is still the maximum. Moreover, the E_{O_v} of $(1\bar{1}02)$-CoO_2 termination is greater than that of the (0001)-LaO_3 surface. Comparing the E_{O_v} in NS state of $(1\bar{1}02)$-LaO and (0001)-LaO_3 facets with previous work [24], it can be found that there is a certain degree of error even if we use the same method and model. It is because that there will be a variety of uncertain spin configurations in the calculation process when we ignore the spin states, since there are a lot of local minimums on the energy surface with different spin configurations. In fact, the above result also represents that the spin states extremely affect surface oxygen vacancies. Therefore, considering the spin states of Co^{3+} ions is an essential role in exploring the surface properties of $LaCoO_3$.

IV. CONCLUSION

We performed DFT+U calculations to study the effect of Co^{3+} spin states on surface stabilities of several low-index terminations of the perovskite $LaCoO_3$. And the E_{O_v} of possible exposed facets is calculated in different spin states. The parameter U is employed to correct the on-site Coulomb and the electron interactions for local d orbitals. It is found that the spin states of Co^{3+} ions in hexagonal-phase $LaCoO_3$ have an important effect on the region of stability diagrams. For the most cases with different spin states and spin configurations of Co^{3+} ions, the $(1\bar{1}02)$-CoO_2 termination can be stabilized in oxygen rich environment, which agrees well with the experimental observation. Moreover, the spin states of Co^{3+} ions can affect surface oxygen vacancy. The higher Co^{3+} spin states give out the lower oxygen vacancy formation energies. Our results reveal that the spin states of Co^{3+} ions should be well considered for studying the properties of $LaCoO_3$ facets.

Supplementary materials: The surface grand potential (Ω) of different terminations in LS, IS (FM, AFM) and HS (FM, AFM) states are displayed, which is expressed as functions of the excess O and Co chemical potentials ($\Delta\mu_{Co}$ and $\Delta\mu_O$).

V. ACKNOWLEDGMENTS

This work was supported by the National Natural Science Foundation of China (No.U1232118, No.21203099), the National Basic Research Program (No.2014CB932403), the Program of Introducing Talents of Disciplines to China Universities (No.B06006), Research Program for Advanced and Applied Technology of Tianjin (No.13JCYBJC36800), Doctoral Fund of Ministry of Education of China (No.20120031120033), Fok Ying Tung Education Foundation (No.151008), and Special Program for Applied Research on Super Computation of the NSFC-Guangdong Joint Fund (the second phase). We appreciate the supports from the National Super-Computing Center at Tianjin and Guangzhou.

[1] E. P. Murray, T. Tsai, and S. A. Barnett, Nature **400**, 649 (1999).
[2] J. Suntivich, K. J. May, H. A. Gasteiger, J. B. Goodenough, and Y. Shao-Horn, Science **334**, 1383 (2011).
[3] J. Suntivich, H. A. Gasteiger, N. Yabuuchi, H. Nakanishi, J. B. Goodenough, and Y. Shao-Horn, Nat. Chem. **3**, 546 (2011).
[4] J. W. Desmond Ng, Y. Gorlin, T. Hatsukade, and T. F. Jaramillo, Adv. Energy Mater. **3**, 1545 (2013).
[5] J. Jung, M. Risch, S. Park, M. G. Kim, G. Nam, H. Y. Jeong, Y. Shao-Horn, and J. Cho, Energy Environ. Sci. **9**, 176 (2016).
[6] C. H. Kim, G. S. Qi, K. Dahlberg, and W. Li, Science **327**, 1624 (2010).
[7] X. G. Li, Y. H. Dong, H. Xian, W. Y. Hernández, M. Meng, H. H. Zou, A. J. Ma, T. Y. Zhang, Z. Jiang, N.

DOI:10.1063/1674-0068/30/cjcp1703035

Tsubaki, and P. Vernoux, Energy Environ. Sci. **4**, 3351 (2011).
[8] K. S. Song, S. K. Kang, and S. D. Kim, Catal. Lett. **49**, 65 (1997).
[9] G. Saracco, G. Scibilia, A. Iannibello, and G. Baldi, Appl. Catal. B **8**, 229 (1996).
[10] Y. M. Choi, D. S. Mebane, M. C. Lin, and M. L. Liu, Chem. Mater. **19**, 1690 (2007).
[11] Y. L. Lee, J. Kleis, J. Rossmeisl, and D. Morgan, Phys. Rev. B **80**, 224101 (2009).
[12] Y. L. Lee, J. Kleis, J. Rossmeisl, Y. Shao-Horn, and D. Morgan, Energy Environ. Sci. **4**, 3966 (2011).
[13] S. O. Choi, M. Penninger, C. H. Kim, W. F. Schneider, and L. T. Thompson, ACS Catal. **3**, 2719 (2013).
[14] M. W. Penninger, C. H. Kim, L. T. Thompson, and W. F. Schneider, J. Phys. Chem. C **119**, 20488 (2015).
[15] S. Khan, R. J. Oldman, F. Corà, C. R. A. Catlow, S. A. French, and S. A. Axon, Phys. Chem. Chem. Phys. **8**, 5207 (2006).
[16] Z. Z. Chen, C. H. Kim, L. T. Thompson, and W. F. Schneider, Surf. Sci. **619**, 71 (2014).
[17] S. G. Zhang, N. Han, and X. Y. Tan, RSC Adv. **5**, 760 (2015).
[18] P. G. Radaelli and S. W. Cheong, Phys. Rev. B **66**, 094408 (2002).
[19] S. M. Zhou, L. F. He, S. Y. Zhao, Y. Q. Guo, J. Y. Zhao, and L. Shi, J. Phys. Chem. C **113**, 13522 (2009).
[20] M. Risch, A. Grimaud, K. J. May, K. A. Stoerzinger, T. J. Chen, A. N. Mansour, and Y. Shao-Horn, J. Phys. Chem. C **117**, 8628 (2013).
[21] S. Mukhopadhyay, M. W. Finnis, and N. M. Harrison, Phys. Rev. B **87**, 125132 (2013).
[22] P. Ravindran, P. A. Korzhavyi, H. Fjellvåg, and A. Kjekshus, Phys. Rev. B **60**, 16423 (1999).
[23] A. Mineshige, M. Inaba, T. Yao, Z. Ogumi, K. Kikuchi, and M. Kawase, J. Solid State Chem. **121**, 423 (1996).
[24] X. Liu, Z. Z. Chen, Y. W. Wen, R. Chen, and B. Shan, Catal. Sci. Technol. **4**, 3687 (2014).
[25] G. Thornton, B. C. Tofield, and A. W. Hewat, J. Solid State Chem. **61**, 301 (1986).
[26] K. Asai, P. Gehring, H. Chou, and G. Shirane, Phys. Rev. B **40**, 10982 (1989).
[27] S. Yamaguchi, Y. Okimoto, and Y. Tokura, Phys. Rev. B **55**, R8666 (1997).
[28] I. A. Nekrasov, S. V. Streltsov, M. A. Korotin, and V. I. Anisimov, Phys. Rev. B **68**, 235113 (2003).
[29] D. P. Kozlenko, N. O. Golosova, Z. Jirk, L. S. Dubrovinsky, B. N. Savenko, M. G. Tucker, Y. Le Godec, and V. P. Glazkov, Phys. Rev. B **75**, 064422 (2007).
[30] W. T. Hong, M. Gadre, Y. L. Lee, M. D. Biegalski, H. M. Christen, D. Morgan, and Y. Shao-Horn, J. Phys. Chem. Lett. **4**, 2493 (2013).
[31] A. M. Ritzmann, M. Pavone, A. B. Muñoz-García, J. A. Keith, and E. A. Carter, J. Mater. Chem. A **2**, 8060 (2014).
[32] G. Kresse and J. Hafner, Phys. Rev. B **47**, 558 (1993).
[33] W. Kohn and L. J. Sham, Phys. Rev. **140**, A1133 (1965).
[34] P. E. Blöchl, Phys. Rev. B **50**, 17953 (1994).
[35] J. P. Perdew, K. Burke, and M. Ernzerhof, Phys. Rev. Lett. **77**, 3865 (1996).
[36] H. J. Monkhorst and J. D. Pack, Phys. Rev. B **13**, 5188 (1976).
[37] A. Chainani, M. Mathew, and D. D. Sarma, Phys. Rev. B **46**, 9976 (1992).
[38] V. I. Anisimov, J. Zaanen, and O. K. Andersen, Phys. Rev. B **44**, 943 (1991).
[39] H. Hsu, K. Umemoto, M. Cococcioni, and R. Wentzcovitch, Phys. Rev. B **79**, 125124 (2009).
[40] L. Wang, T. Maxisch, and G. Ceder, Phys. Rev. B **73**, 195107 (2006).
[41] C. L. Ma and J. Cang, Solid State Commun. **150**, 1983 (2010).
[42] F. Bottin, F. Finocchi, and C. Noguera, Phys. Rev. B **68**, 035418 (2003).

DOI:10.1063/1674-0068/30/cjcp1703035